

Thickness Dependent Surface Topography, Magnetic Properties and Magnetic Domain Structure of Amorphous FeTaC Thin Films

Camelia Das¹, Jumal Das¹, Thiruvengadam Vijayabaskaran², Subhankar Bedanta², Abhishek Talapatra³, Jyoti Ranjan Mohanty³ and Perumal Alagarsamy^{1*}

¹Department of Physics, Indian Institute of Technology Guwahati, Guwahati-781039, India

²School of Physical Sciences, National Institute of Science Education and Research, Bhubaneswar-751005, India

³Department of Physics, Indian Institute of Technology Hyderabad, Hyderabad-502285 India

Abstract

We report systematic investigation of thickness dependent surface topography, magnetic properties and magnetic domain structures of amorphous $\text{Fe}_{80}\text{Ta}_8\text{C}_{12}$ (x nm) films with $x=5-100$ nm. All the as-deposited films fabricated directly on thermally oxidized Si substrate at ambient temperature using magnetron sputtering technique exhibit amorphous structure. The structural studies reveal that island-like structure in ultra-thin films transforms into continuous one with increasing $x>10$. In addition, the average surface roughness increases with increasing x , but without any systematic dependency on x . Room temperature magnetic properties illustrate that the paramagnetic nature observed for films with $x<10$ changes into ferromagnetic one with rectangular loops having high remanence ratio ($M_r/M_s>97\%$), low coercivity ($H_c<1.77$ kA/m), low saturation field ($H_s<2.2$ kA/m) and simple magnetization reversal behavior for x up to 40 nm. Upon increasing $x \geq 50$, the loop shape again changes into transcritical one with increased $H_c (>3.5$ kA/m) and $H_s (>40$ kA/m) and reduced $M_r/M_s (<45\%)$. The magnetic domain studies not only reveal that the domains change from in-plane magnetization to dense stripe domain pattern with increasing x due to enhancement of effective magnetic anisotropy caused by stress quenched in during deposition, but also confirm that films with $12<x<40$ exhibit in-plane magnetization with uniaxial anisotropy. High temperature thermomagnetization reveal a clear magnetic phase transition from ferromagnetic to paramagnetic state at relatively higher temperature of about 530 K. The observed results are elucidated on the basis of enhanced effective magnetic anisotropy, change in the magnetic domain structure and magnetic disorder with increasing FeTaC film thickness.

Keywords: Amorphous materials; Magnetic materials; Thin films; Sputtering; Atomic force microscopy

Introduction

A key trend in recent science and technology is the exploitation of phenomena occurring at length scales between 1 and 500 nm, which has led to the emergence of new fields in nanoscale science. During the last few decades, the tendency to miniaturize the dimensions of electronic devices has created a demand for new materials and new methods for their production. Thin films of various magnetic alloys play a major role in miniaturization of integrated circuits in magnetoelectronic devices. Hence, searches for suitable magnetic thin films with enhanced soft magnetic properties (high saturation magnetization (M_s), low coercivity (H_c), low saturation field (H_s), large relative permeability, controllable magnetic anisotropy and good thermal stability) have been carried out widely not only for practical applications in modern magnetic devices such as magnetic passives, energy transferring devices, soft underlayer in perpendicular magnetic recording media, magnetic flux amplifier, high-density magnetic recording read heads and magnetoresistive random access memories, flexible spintronics, but also for gaining fundamental knowledge on low-dimensional systems [1-10].

In order to obtain soft magnetic thin films, it is very much essential to understand the correlation between the structural and magnetic properties so that a well-defined magnetic domain structure can be achieved in magnetic thin films. Therefore, extensive studies have been carried out since past two decades on various amorphous single-layer thin films such as FeCuNbSiB [10,11], FeAlSi [12], CoNbZr [13], FeTa(C)N [14,15], FeTaC [16,17], Fe-Zr-N [18], CoTaZr [19] and CoFeB [2,3,20]. However, it has been revealed from a careful review of the literature that the soft magnetic properties of the magnetic films display a strong dependence on the film thickness and the

growth conditions of the films. Interestingly, the thickness dependent magnetic properties of the films do not show unique behaviour, but depend strongly on the constituent elements [1,21-24]. In addition, the equilibrium magnetic domain structure in magnetic films is governed by the competition of various energy terms (exchange, dipolar and anisotropy energies) and conversely the orientation of magnetization is determined by the effective anisotropy constant. These types of soft magnetic thin films also display spin-reorientation transition from in-plane single domain like state to out-of-plane multi-domain state or vice-versa with increasing film thickness or change in the substrate temperature during sample preparation [25-28]. As the use of amorphous magnetic films in different functional devices becomes more pervasive, it is essential to explore the emergence of effective magnetic anisotropy and approaches to minimize out-of-plane magnetic component to realize soft magnetic properties in thin films. Nevertheless, most of the published results narrate thickness dependent studies at room temperature from the application point of view without any detailed or systematic investigations aiming at understanding the surface topography and magnetic nature of the films at different thicknesses. Hence, in this report, we have investigated the

***Corresponding author:** Perumal Alagarsamy, Department of Physics, Indian Institute of Technology Guwahati, Guwahati-781039, India, Tel: +91-361-258-2714; Fax: +91-361-2690762; E-mail: alagarsamy.perumal@gmail.com

Received May 09, 2018; Accepted May 22, 2018; Published June 02, 2018

Citation: Das C, Das J, Vijayabaskaran T, Bedanta S, Talapatra A, et al. (2018) Thickness Dependent Surface Topography, Magnetic Properties and Magnetic Domain Structure of Amorphous FeTaC Thin Films. J Material Sci Eng 7: 455. doi: [10.4172/2169-0022.1000455](https://doi.org/10.4172/2169-0022.1000455)

Copyright: © 2018 Das C, et al. This is an open-access article distributed under the terms of the Creative Commons Attribution License, which permits unrestricted use, distribution, and reproduction in any medium, provided the original author and source are credited.

effect of thickness on the surface topography, magnetic properties and magnetic domain structure of amorphous Fe₈₀Ta₈C₁₂ thin films.

Experimental Details

Amorphous Fe₈₀Ta₈C₁₂ (FeTaC) alloy single-layer thin films with different thicknesses ($x=5 - 100$ nm) were deposited directly on thermally oxidized Si substrate using DC magnetron sputtering technique at ambient temperature. The base pressure of the chamber was better than 1×10^{-4} Pa and the sputtering Ar gas pressure was optimized at 1.33 Pa. The deposition rate was pre-calibrated using ex-situ surface profilometer (Veeco, Dektak 150 model) and found to be 0.41 Å/s for the deposition of FeTaC. Amorphous nature of the as-deposited films was confirmed by X-ray diffraction (XRD) recorded using a high-power X-ray diffractometer (Rigaku TTRAX III, 18 kW) with Cu-K_α radiation ($\lambda=1.541$ Å) and transmission electron microscopy (TEM, Jeol 2100 and Technai G2 F20) techniques. X-ray reflectivity (XRR) technique was used to evaluate various film parameters such as film thickness, surface roughness, etc. Simultaneous atomic force microscopy (AFM) and magnetic force microscopy (MFM) analyses were performed to study the topographic features and local magnetic domains (Bruker Dimension Icon). MFM was performed in dual-pass lifting mode with commercially available CoCr-coated tips, which were magnetized along the tip axis and therefore sensitive to stray field gradients from out-of-plane oriented domains or the out-of-plane components of domains oblique to the surface. The domain images were acquired at the zero-field state. Magnetic properties were characterized by using vibrating sample magnetometer (VSM, LakeShore Model 7410) by performing magnetic hysteresis loops ($M-H$) along the film plane. Magnetic domain images and Kerr loops were obtained using magneto-optic Kerr effect (MOKE) microscopy (Evico Magnetics Ltd, Germany) technique. Imaging was performed using linearly polarized light with white LED as source. Magnetic domain images were observed in both branches of hysteresis cycle in longitudinal MOKE mode. Hysteresis accompanied by simultaneous imaging has been performed for magnetic fields applied along various in-plane directions [easy (0°) and hard (90°) axes].

Results and Discussion

Figure 1 shows typical XRD patterns for FeTaC films with $x=50$ and 100 nm, bright-field plane-view TEM image, selected area electron diffraction (SAED) pattern and high-resolution TEM (HRTEM) image for 100 nm thick FeTaC film. It could be clearly seen that as-deposited films exhibit only broad peaks at around $2\theta=44^\circ$ without any sharp peaks peculiar to any other crystalline phases. This confirms the amorphous nature in the as-deposited films. The XRD peak observed at $2\theta=33.05^\circ$ represents Si(200) peak due to thermally oxidized Si substrate [29]. The amorphous nature is also confirmed from TEM studies, which reveal the existence of plane and even contrast microstructure without any local lattice fringes and halo diffraction ring, respectively.

Since the magnetic properties of the thin films strongly depend on the film thickness, it is very much essential to study the actual film thickness and associated roughness as a function of thickness. XRR is one of the non-destructive techniques widely used to evaluate various film parameters such as film thickness, film density, surface/interface roughness, etc. Hence, the XRR curves are recorded for the as-deposited FeTaC films and the typical curves are presented in Figure 2 for selected thicknesses. The interference pattern (open circles) with clear oscillation peaks is observed for all the as-deposited films. With increasing 2θ , the oscillation intensity decreases and attains the same level as the noise in the higher angle region. With increasing x ,

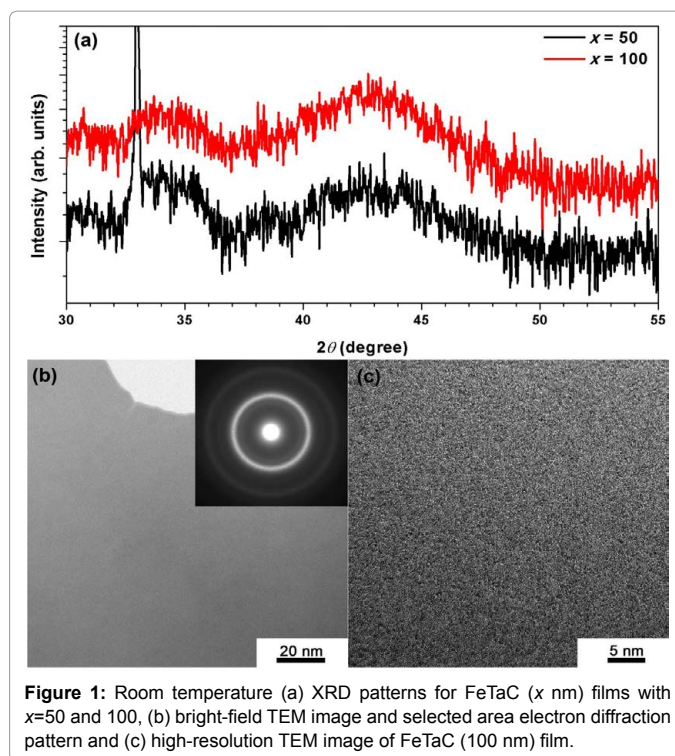


Figure 1: Room temperature (a) XRD patterns for FeTaC (x nm) films with $x=50$ and 100, (b) bright-field TEM image and selected area electron diffraction pattern and (c) high-resolution TEM image of FeTaC (100 nm) film.

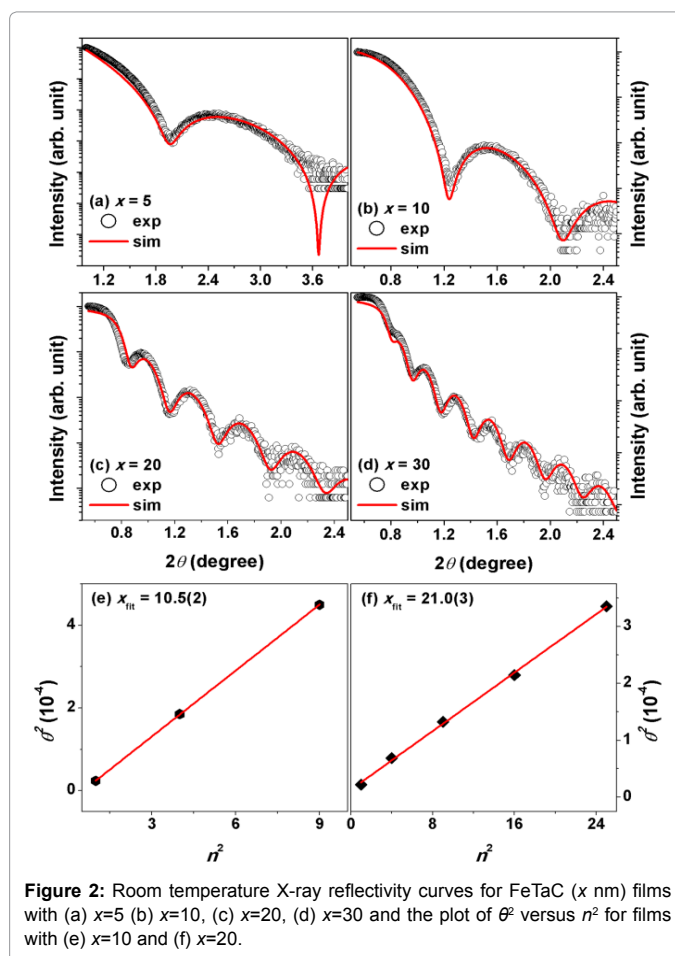


Figure 2: Room temperature X-ray reflectivity curves for FeTaC (x nm) films with (a) $x=5$ (b) $x=10$, (c) $x=20$, (d) $x=30$ and the plot of θ^2 versus n^2 for films with (e) $x=10$ and (f) $x=20$.

the number of oscillation peaks increases and peak width decreases systematically. To understand the changes in the XRR curves with increasing x carefully, fitting of the XRR curves is preceded by a pattern fitting process between the measured and simulated XRR pattern using GlobalFit software offered by Rigaku. During the analysis, a layered sample model, consists of two simulated layers: (i) a thick SiO_2 layer and (ii) a layer of FeTaC film, is constructed to generate a simulated reflectivity curves. The thickness of the films, interfacial and surface roughnesses, and density of the materials are treated as free fitting parameters to obtain best fits using Globalfit software. As shown in Figure 2, the solid lines representing the simulated data using the layered sample model show decent fit to the experimental data and the extracted parameters from the fit are listed in the Table 1. While the thickness determined from the fit merely matches with the experimental value, the surface roughness of the FeTaC film does not show any good correlation with the thickness. Nevertheless, the surface roughness increases slightly with increasing x . This could be attributed to the stress, induced in the film during the deposition at a faster deposition rate to form amorphous structure, which modifies the surface topography with increasing x . The simulated film thickness is further reconfirmed analytically by using Savitzky-Golay (SG) algorithm as described in eqn. (1) [30].

$$\theta^2 = \frac{\lambda^2}{4x^2} n^2 + 2\delta \quad (1)$$

where θ is the Bragg angle, λ ($=1.541 \text{ \AA}$) is the X-ray wavelength of the Cu- K_α radiation, x is the thickness of the film, n is the number of XRR maxima and δ is the dispersion factor of X-ray beam. The values of θ and n are extracted from the XRR curves and plotted as θ^2 vs n^2 typically for FeTaC films with $x=10$ and 20 nm in Figure 2e and 2f, respectively. The experimental data show almost linear behaviour and the fit to the data using eqn.(1) provides the values of 2δ from the intercept and $\lambda^2/(4x^2)$ from the slope. Subsequently, x is determined from the slope and listed in Table 1. The thickness calculated from the SG algorithm is found to be slightly higher than the estimated thickness, but within the error values. This may be possibly related to the difficulties in identifying the exact peak position from the broad spectrum of the XRR curves or due

to surface roughness. Nevertheless, the values of x determined from layered sample model using Globalfit and SG algorithm are in close agreement with the predicted thickness using pre-calibrated deposition rate.

To study the effect of thickness on the surface topography of the films, we have investigated the topography of the films using AFM and shown in Figure 3. The following features are observed from the AFM images: (i) FeTaC film with $x=5$ nm forms island like structure along with the existence of very fine nanosized grains of less than 10 nm, which are sparsely distributed. Therefore, the resistance of the film is found to be very high in the range of $10^5 \Omega$. (ii) With increasing $x>5$ nm, all the films display a very clear uniform surface with grain morphology and the grain density increases with increasing x . This reduces the resistance of the films largely down to below 100Ω . (iii) The extracted values of surface roughness, summarized in Table 1, clearly suggest that although the surface roughness increases significantly with increasing x , it does not show any systematic variation with increasing x . These results are in good agreement with those results obtained from XRR analysis using Globalfit software.

Figure 4 depicts room temperature normalized $M-H$ loops measured along the film plane for FeTaC film with different thicknesses ($x=5-100$ nm). The extracted magnetic parameters such as H_C , H_S , the nucleation field (H_N) and remanence ratio (M_R/M_S , where M_R is remanence magnetization) from the $M-H$ loops are plotted as a function of x in Figure 5. It is observed that (i) FeTaC film with $x=5$ nm shows a very weak magnetic signal (paramagnetic) with a noisy background. (ii) With increasing x to 10 nm, the film exhibits a clear hysteresis behaviour, which needs a higher applied magnetic field to saturate the film's magnetization. (iii) On further increasing x up to 40 nm, all the films depict rectangular shaped loops with high M_R/M_S of more than 97% and lower H_S (<2.2 kA/m). H_C and H_N increase progressively from 0.42 kA/m to 1.77 kA/m and from -0.3 kA/m to -1.67 kA/m with increasing x from 12 to 30 nm, respectively and then decreases slightly to 1.43 kA/m and -1.35 kA/m for $x=40$ nm film. (iv) The loop shape changes drastically into different nature upon increasing $x \geq 50$ nm,

FeTaC film thickness (x nm)	Simulated XRR results		Analytical results thickness (x nm)	AFM surface roughness (nm)
	Thickness (x nm)	Surface roughness (nm)		
5	4.9 (3)	0.45 (2)	5.3 (2)	0.38 (3)
10	9.4 (6)	0.47 (3)	10.5 (2)	0.53 (2)
20	19.8 (3)	0.55 (2)	21.0 (3)	0.60 (2)
30	29.3 (7)	0.61 (2)	30.7 (2)	0.53 (1)
50	49.5 (5)	0.72 (3)	50.3 (2)	0.69 (3)
70	69.4 (7)	0.69 (3)	70.6 (3)	0.74 (3)
100	99.1 (9)	0.75 (2)	100.2 (4)	0.80 (2)

Table 1: Comparisons of actual thickness and thickness obtained from simulation and analytical results from XRR pattern of FeTaC ($x=5-100$ nm) films. The average surface roughness estimated from both simulation and AFM topography is also included.

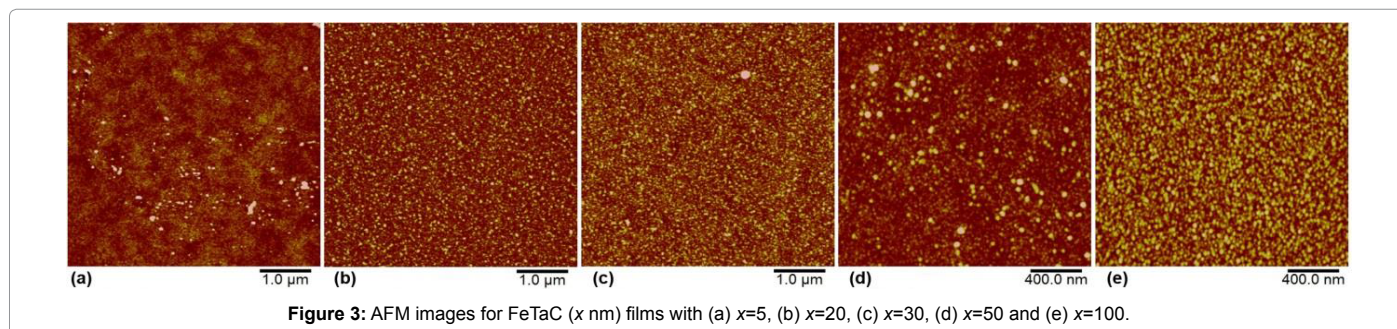


Figure 3: AFM images for FeTaC (x nm) films with (a) $x=5$, (b) $x=20$, (c) $x=30$, (d) $x=50$ and (e) $x=100$.

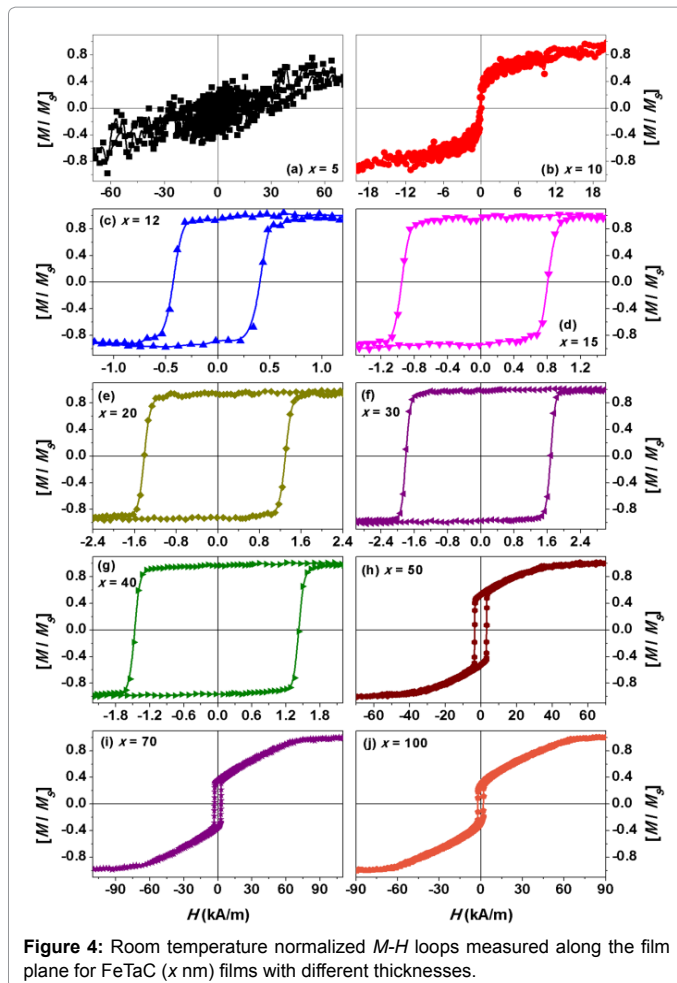


Figure 4: Room temperature normalized M - H loops measured along the film plane for FeTaC (x nm) films with different thicknesses.

i.e., the loop consists of two distinct magnetization reversal phases: (a) in-plane magnetic components, which reverse quickly near to H_c and (b) perpendicular components, which rotate continuously under the application of magnetic field before attaining saturation magnetization. As a result, the latter one produces a linear variation of magnetization before the saturation and one needs considerably a large H_s to saturate film's magnetization (> 40 kA/m). This type of loop shape has been often specified as transcritical loop [25,26,31-33]. (v) Therefore, H_c increases suddenly to 3.5 kA/m and then decreases almost linearly at a rate of 28.6 A/(m-nm) for x up to 100 nm. Similarly, H_s also increases rapidly to 64.7 kA/m with increasing x to 70 nm and then tends to saturate for $x=100$ nm film. (vi) In addition, the magnitude of magnetization reversing close to H_c decreases significantly and the region of linear variation of magnetization increases largely with increasing x . This causes a large reduction in M_r/M_s down to 30% for $x=100$ nm film. These results clearly suggest that the magnetic properties of FeTaC films at room temperature strongly depend on x , i.e., (i) FeTaC films with $x < 10$ nm show paramagnetic nature at room temperature, (ii) a clear ferromagnetic behaviour with rectangular shaped loop is observed when $12 \text{ nm} \leq x \leq 40$ nm, and (iii) the rectangular shaped loop transforms into transcritical one for $x \geq 50$ nm.

The observation of paramagnetic nature in ultra-thin films could be interpreted to the growth morphology of island-like structure during the initial growth stage of the films. With increasing x , the island like structure turns out to be continuous. This develops in-plane anisotropy

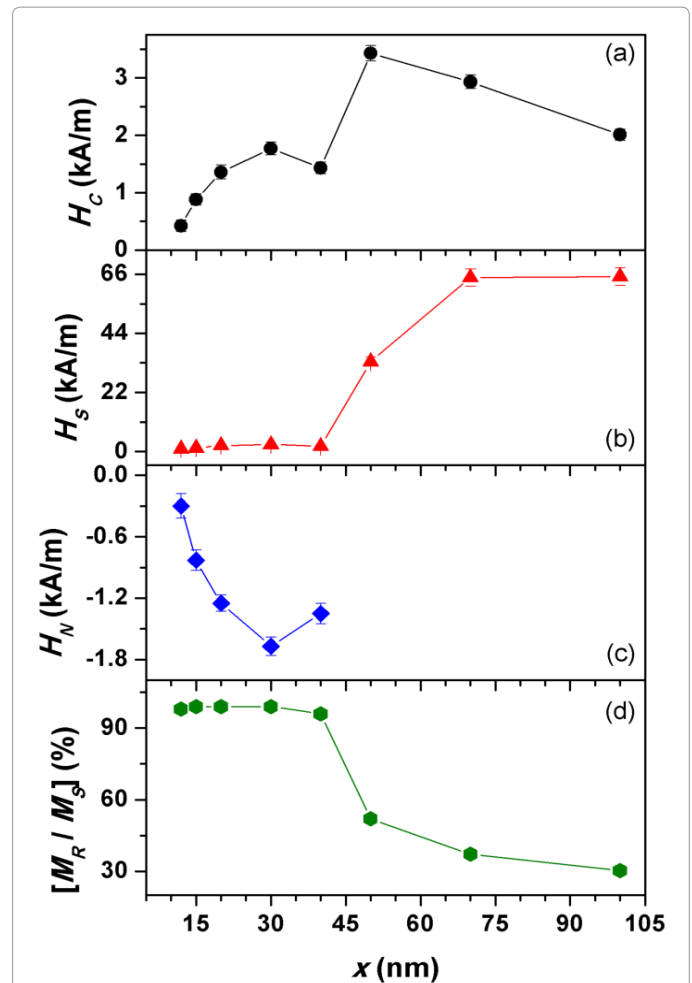


Figure 5: The variations of (a) H_c , (b) H_s , (c) H_n and (d) $[M_r/M_s]$ as a function of thickness of FeTaC (x nm) films.

in the films caused by the formation of aligned ferromagnetic atom pairs due to their strong magnetic exchange coupling during deposition process. Since the films are deposited at a faster deposition rate to form amorphous structure, the stress quenched in the films during deposition increases progressively with increasing x [25,31]. Hence, H_c , H_s and H_n increase gradually with increasing x up to 30 nm. Upon increasing x beyond critical value (50 nm in the presently investigated films), the spin-reorientation transition from in-plane magnetization to dense stripe domain occurs due to stress induced effective magnetic anisotropy (K_{eff}). In order to elucidate the nature of magnetic domains, the magnetic domain structure is investigated using MFM and depicted in Figure 6. The films with $x \leq 40$ nm display almost no features visible through MFM, which is sensitive only to the magnetic field generated by the sample magnetization directed out-of-plane to the sample surface. This could be attributed to the existence of in-plane magnetic domains, which characterize soft magnetic behaviour in these films as evidenced from Figure 4. On the other hand, higher thickness FeTaC films ($x > 50$ nm) are elucidated by the presence of magnetic dense stripe domains with a component of the magnetization vector directed perpendicular to the film plane. Therefore, these films exhibit transcritical loop due to two distinct magnetization phases. The width of the stripe domains determined by a proper Fast Fourier Transform analysis of the MFM image is found to be about 74 nm. This is in close agreement with the earlier reports on similar amorphous systems [18,25,31,34-37].

Although FeTaC (50 nm) film unveiled transcritical like loop (Figure 4h), the MFM image depicts random nucleation of perpendicular magnetic component without a clear dense stripe domain pattern. This could be attributed to presence of large in-plane magnetic component and development of progressive perpendicular component in the film. These results confirm that the magnetic domains transform from in-plane orientation of magnetization to stripe domain at a critical thickness of 50 nm.

To study the nature of in-plane magnetic domains in details, we have simultaneously obtained Kerr loops and magnetic domain images along the film planes using MOKE microscopy. Figure 7 depicts the room temperature Kerr loops measured along the film planes and magnetic domain images for FeTaC (20 nm) film. It is clearly evident that the film displays rectangular shaped loop in one direction (easy-axis direction in the plane (0°)) and nearly flat type loop characterized by reduced remanence in another direction (hard-axis direction in the plane (90°)). The values of H_s in both the measurement directions are found to be nearly the same. In addition, the magnetic field required to switch the magnetization along the easy-axis from one direction to another direction is observed to be quite low (<0.25 kA/m). From the VSM results (Figure 4e), the magnetic field required to switch the magnetization from one direction to another direction is found to be about 0.4 kA/m, which is slightly larger than the one obtained from MOKE microscopy. This could be possibly related to the contribution from the finite edges of the sample used in VSM measurement. The magnetic domain images obtained along the easy-axis display a rapid switching of large-sized magnetic domains due to domain wall motion. On the other hand, the magnetic domain images obtained along the hard-axis reveal no clear domain reversal process due to coherent like magnetization rotation process. This supports the existence of in-plane uniaxial magnetic anisotropy in the films. Accordingly, the value of K_U is determined using eqn. (2):

$$K_U = \frac{M_s H_K}{2} \quad (2)$$

where, H_K is the anisotropy field. The determined values of K_U listed in Table 2 show a continuous increase up to $x=30$ nm and then decrease slightly for $x=40$ nm. On further increasing x (≥ 50 nm), the

stress induced magnetic disorder destabilizes the uniaxial anisotropy, which in turn enhances K_{eff} to develop magnetic dense stripe domain. To analyse the development of K_{eff} at higher x and the corresponding magnetic domain configuration, dense stripe domain model proposed by Craus et al. [18,38] following the original model proposed by Mayurama et al. [32] and Alvarez-Padro et al. [33] is used to calculate K_{eff} . The schematic of the dense stripe domain model is demonstrated in Figure 8. According to this model, the spins in the bulk domains make an angle θ_1 with the surface and the closure domain spins on the surface make an angle θ_2 with the long axis of the stripes. The values of θ_1 can be calculated either from Mössbauer data or from the remanence magnetization data measured using the VSM under the condition that the magnetization in the closure domains remains perpendicular to the direction of the applied magnetic field such that $\theta_2 = \pi/2$. The values of θ_1 , playing a crucial role on the magnetic properties of the thicker films, varies between 0 and 90° depending on the values of M_R/M_S [38]. Moreover, there exists a critical film thickness (x_c), as given eqn. (3), beyond which dense stripe domain appears due the continuous development of stress in as-deposited film.

$$x_c = \frac{2\pi}{\left(1 - \frac{\mu_0 M_s H_s}{2K_{eff}}\right)} \sqrt{\frac{A}{K_{eff}}} \quad (3)$$

where x_c is critical thickness above which the dense stripe domain appears, A is exchange stiffness constant taken as 10×10^{-12} J/m and μ_0 is absolute permeability. The existence of stripe domains in critical thickness films depends strongly on the values of M_s and K_{eff} [32,39]. Note that the values of M_s and H_s could be extracted directly from the $M-H$ loops. Since we observed the existence of stripe domain structure in the presently investigated FeTaC films, the values of K_{eff} are determined by substituting the values of H_s , M_s , A and x_c in eqn. (3). Similarly, the domain wall width (w) is calculated by assuming a Landau domain structure [40], which is compatible when the sample thickness is larger than $\sqrt{A/K_{eff}}$, as in the present case, using:

$$w = 2 \sqrt{2x} \sqrt{\frac{A}{K_{eff}}} \quad (4)$$

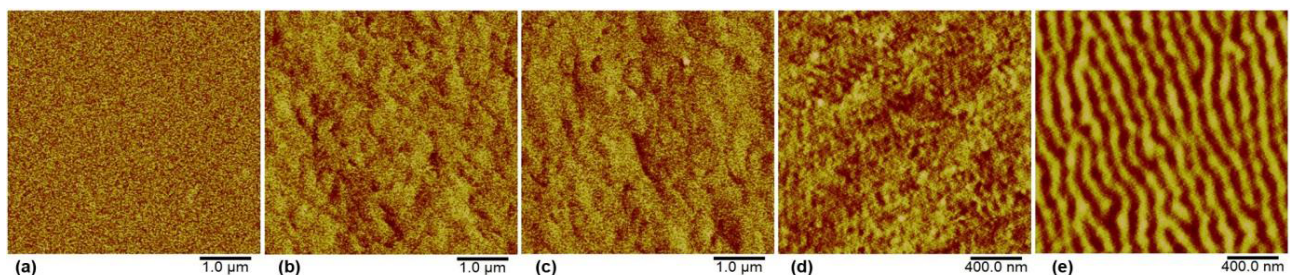
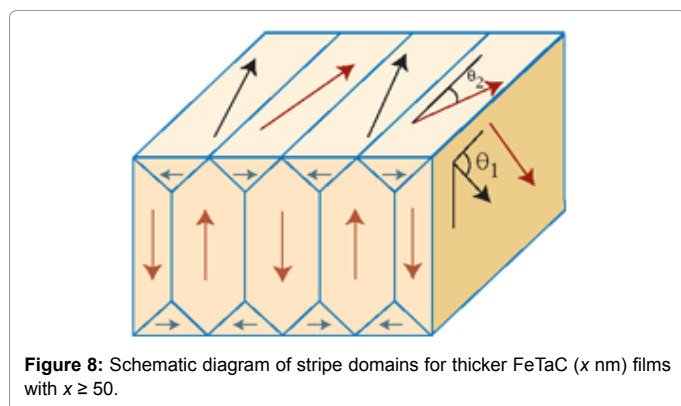
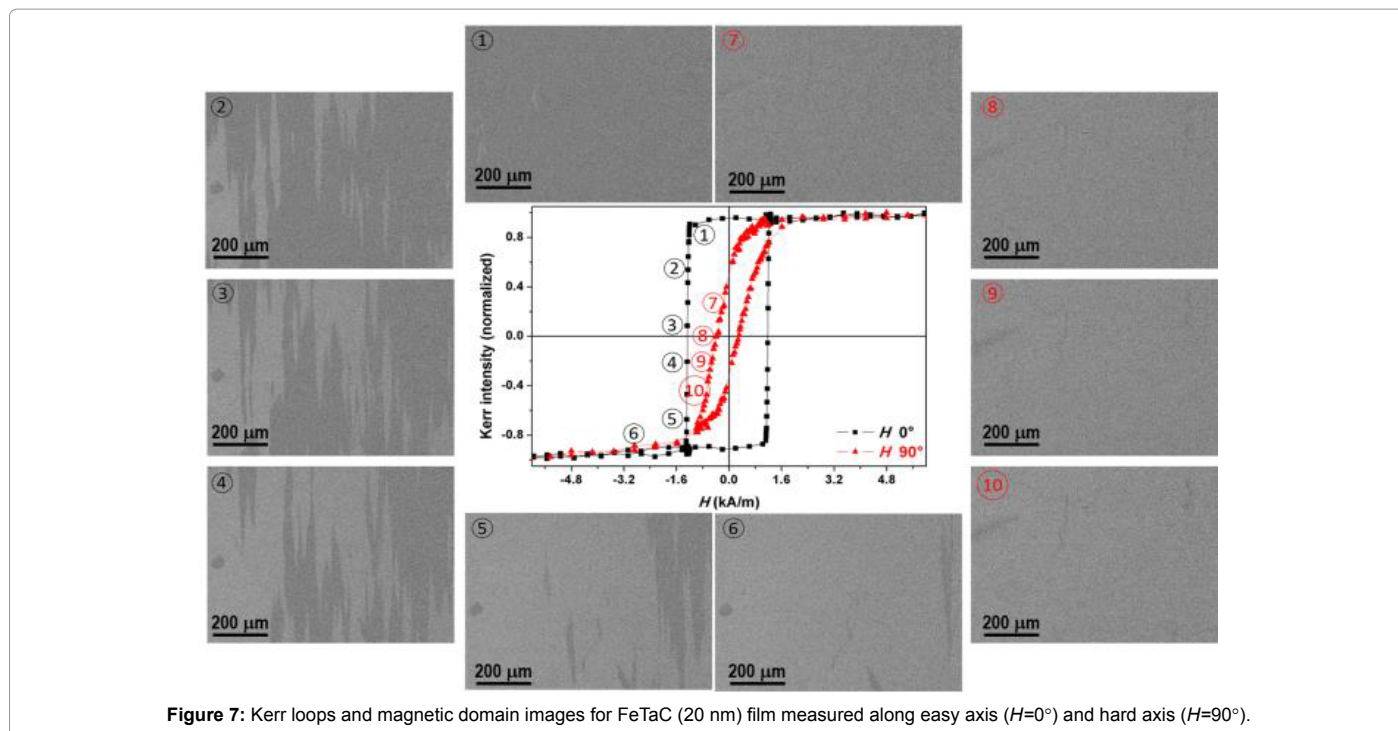


Figure 6: MFM images obtained at zero-field state for FeTaC (x nm) films with (a) x=5, (b) x=20, (c) x=30, (d) x=50 and (e) x=100.

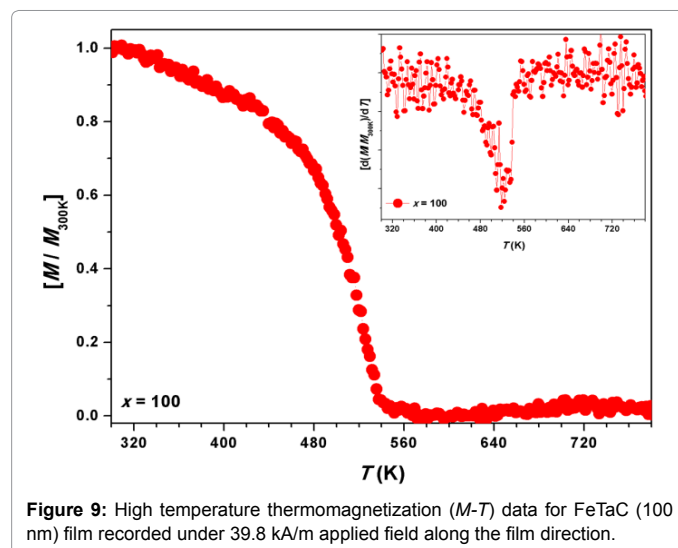
FeTaC thickness (x nm)	H_K (or) H_s (kA/m)	K_U (J/m ³)	$\mu_0 M_s$ (mT)	K_{eff} (J/m ³)	w (nm)	(θ_1)
12	1.03 (5)	147.7 (3)	265 (2)	-	-	-
20	2.31 (7)	449.5 (4)	389 (3)	-	-	-
30	2.63 (6)	646.8 (5)	492 (3)	-	-	-
40	1.99 (4)	461.2 (5)	463 (4)	-	-	-
50	33.44 (5)	-	594 (3)	$1.77 (2) \times 10^5$	54.8 (3)	43.2 (3)
70	64.73 (6)	-	415 (2)	$1.83 (3) \times 10^5$	64.3 (1)	56.6 (4)
100	65.13 (8)	-	501 (2)	$1.89 (2) \times 10^5$	76.3 (2)	62.7 (2)

Table 2: The thickness dependent H_K , H_s , K_U , $\mu_0 M_s$, K_{eff} , w and θ_1 for FeTaC films.



The determined values of K_{eff} , θ_1 and w are listed in Table 2 for $x \geq 50$ nm films. The domain wall width determined from this model and MFM image is in good agreement with each other. In addition, the obtained values of K_{eff} are in good agreement with those values reported for other similar amorphous systems [28,41,42].

In order to understand the stability of ferromagnetic phase in FeTaC film, high temperature $M-T$ data are recorded at a constant applied field of 39.8 kA/m. Figure 9 illustrates the normalized $M-T$ data above room temperature for FeTaC (100 nm) film. It could be clearly seen from the figure that the film exhibits an incessant decrease in magnetization with increasing temperature up to 540 K and then nearly constant up to 720 K. This is correlated to the magnetic phase transition of the amorphous phase from ferromagnetic to paramagnetic state. Curie temperature (T_c) determined from the thermal derivative of $M-T$ data is found to be about 525 ± 3 K. This is almost similar to the one obtained for CoFeB alloys confirming thermally stable magnetic phase in amorphous FeTaC film [42,43]. Therefore, the results shown in this paper reveal that the magnetic properties of amorphous FeTaC (x nm) films depend strongly on x . It also provides a comprehensive



study of optimizing the soft magnetic properties and magnetic domain structure with respect to film thickness.

Conclusion

We have fabricated amorphous $Fe_{80}Ta_8C_{12}$ single-layer films with different thicknesses directly on thermally oxidized Si substrate using DC magnetron sputtering technique at ambient temperature and characterized their structural and magnetic properties, and domain structures. The structural studies using XRD and TEM confirmed the amorphous nature of the as-deposited films, while the characterization using XRR and AFM revealed that the average surface roughness increased with increasing film thickness, but without any systematic dependence on thickness. Room temperature magnetic properties showed that with increasing film thickness, the paramagnetic nature

of the films for thickness below 10 nm changed into ferromagnetic one with simple magnetization reversal for thickness upto 40 nm and transformed into transcritical one above 50 nm thickness. Therefore, coercivity and saturation field increased largely. This was correlated to the change in the magnetic domain structure from in-plane magnetization to dense stripe domain pattern due to enhancement of effective magnetic anisotropy caused by the stress quenched in during deposition at a faster deposition rate to form amorphous structure. The magnetic domain structure analysis revealed that low thickness FeTaC films exhibited in-plane magnetic domains with uniaxial in-plane magnetic anisotropy. High temperature thermo magnetization data revealed the magnetic phase transition from ferromagnetic to paramagnetic state at relatively higher temperature of about 525 K. The observed results are discussed on the basis of development of effective magnetic anisotropy, change in the magnetic domain structure and magnetic disorder with increasing FeTaC film thickness.

Acknowledgement

This work is financially supported by the Board of Research in Nuclear Sciences (BRNS), Department of Atomic Energy (DAE), Mumbai, India (37(3)/14/29/2015/BRNS). Infrastructure facilities provided by DST, New Delhi (SR/S2/CMP-19/2006, SR/FST/PII-020/2009) and Defence Research and Development Organization, New Delhi (ERIP/ER/0900363/M/01/1185) are gratefully acknowledged.

References

- Masood A, McCloskey P, Mathúna C, Kulkarni S (2018) Co based amorphous thin film with on silicon with soft magnetic properties. *AIP Adv* 8: 056109.
- Vemulkar T, Mansell R, Pacheco AF, Cowburn RP (2016) Towards flexible spintronics: Perpendicularly magnetized synthetic antiferromagnetic thin films and nanowires on polyimide substrates. *Adv Func Mater* 26: 4704.
- Hao Z, Yuan LY, Yin YM, Bao Z, Guang Y, et al. (2015) Tuning the magnetic anisotropy of CoFeB grown on flexible substrates. *Chinese Physics B* 24: 077501.
- Coey M, Lewis LH, Ma BM, Schrefl T, Schultz L, et al. (2014) *Advanced hard and soft magnetic materials*. Cambridge University Press.
- Chen CW (2013) *Magnetism and metallurgy of soft magnetic materials*. Dover Publications, Inc., New York.
- Seki TO, Takahashi YK, Hono K (2008) Microstructure and magnetic properties of FePt-SiO₂ granular films with Ag addition. *J Appl Phys* 103: 023910.
- Piramanayagam SN (2007) Perpendicular recording media for hard disc drives. *J Appl Phys* 102: 011301.
- Khizroev S, Litvinov D (2004) Perpendicular magnetic recording: Writing process. *J Appl Phys* 95: 4521.
- Hartmann U (1999) *Magnetic multilayers and giant magnetoresistance: Fundamentals and industrial applications*. Springer, New York.
- Naoe M, Matsumiya H, Ichihara T, Nakagawa S (1998) Preparation of soft magnetic films of nanocrystalline Fe-Cu-Nb-Si-B alloy by facing targets sputtering. *J Appl Phys* 83: 6673.
- Fujii I, Shima T, Takanashi K (2006) Magnetic properties of L₁₀ ordered FePt films prepared on a Fe-Si-B-Nb-Cu soft magnetic underlayer. *Mater Trans* 47: 47.
- Tate BJ, Parmer BS, Todd I, Davies HA, Gibbs MRJ, et al. (1998) Soft magnetic properties and structures of nanocrystalline Fe-Al-Si-B-Cu-Nb alloy ribbons. *J Appl Phys* 83: 6335.
- Hirayama Y, Kikukawa A, Honda Y, Shimizu N, Futamoto M (2000) Low noise performance of CoCrPt single-layer perpendicular magnetic recording media. *IEEE Trans Magn* 36: 2396.
- Wei VF, Wu D, Zheng D, Ma B, Yang Z (2000) Investigation of RF-sputtered Fe-Ta-N thin films. *Mater Sci Engg B* 68: 156.
- Jiang RF, Lai CH (2005) Origin of the anisotropy in soft nanocrystalline FeTaCN films. *J Appl Phys* 97: 10N302.
- Tanahashi K, Kikukawa A, Takahashi Y, Hosoe Y, Futamoto M (2002) Low-noise FeTaC underlayer for double-layered perpendicular recording media. *J Magn Mater* 242: 325.
- Samantaray B, Singh AK, Banerjee C, Barman A, Perumal A, et al. (2016) Perpendicular standing spin wave and magnetic anisotropic study on amorphous FeTaC films. *IEEE Trans Magn* 52: 2003104.
- Craus CB, Chezan AR, Siekman MH, Lodder JC, Boerma DO, et al. (2002) Stripe domains in Fe-Zr-N nanocrystalline films. *J Magn Mater* 240: 423.
- Lee DW, Wang SX (2006) Multiple magnetic resonances in permeability spectra of thick CoTaZr films. *J Appl Phys* 99: 08F109.
- Guerrero MG, Prieto JL, Ciudad D, Sanchez P, Aroca C (2007) Engineering the magnetic properties of amorphous with multilayers of variable anisotropy direction. *Appl Phys Lett* 90: 162501.
- Masood A, McCloskey P, Mathúna C, Kulkarni S (2017) Controlling the competing magnetic anisotropy energies in FineMET amorphous thin films with ultra-soft magnetic properties. *AIP Adv* 7: 055208.
- Huang MQ, Hsu YN, McHenry E, Laughlin DE (2001) Soft magnetic properties of nanocrystalline amorphous HITPERM films and multilayers. *IEEE Trans Magn* 37: 2239.
- Nakamura F, Hikosaka T, Tanaka Y (2001) Low noise multi-layered FeAlSi soft magnetic films for perpendicular magnetic recording media. *J Magn Mater* 235: 64.
- Mapps DJ, Akhter MA, Pan G (1991) CoNbFe soft magnetic thin-film backlayers for glass computer disks. *J Appl Phys* 69: 5178.
- Sharma P, Kimura H, Inoue A, Arenholz E, Guo JH (2006) Temperature and thickness driven spin-reorientation transition in amorphous Co-Fe-Ta-B thin films. *Phys Rev B* 73: 052401.
- Li XW, Song C, Yang J, Zeng F, Geng KW, et al. (2007) Thickness-dependent magnetization reversal in CoZrNb amorphous films. *J Magn Mater* 315: 120.
- Coisson M, Celegato F, Olivetti E, Tiberto P, Vinai F, et al. (2008) Stripe domain and spin reorientation transition in Fe₇₈B₁₃Si₉ thin films produced by rf sputtering. *J Appl Phys* 104: 033902.
- Coisson M, Appino C, Celegato F, Magni A, Tiberto P, et al. (2008) Magnetization processes in sputtered FeSiB thin films. *Phys Rev B* 77: 214404.
- Cho MH, Ko DH, Choi YG, Jeong K, Lyo IW, et al. (2001) Structural and electrical characteristics of Y₂O₃ films grown on oxidized Si(100) surface. *J Vac Sci Technol A* 19: 192.
- Serafinczuk J, Pietrucha J, Schroeder G, Gotszalk TP (2011) Thin film thickness determination using X-ray reflectivity and Savitzky-Golay algorithm. *Optica Applicata XLI*: 315.
- Coisson M, Vinai F, Tiberto P, Celegato F (2009) Magnetic properties of FeSiB thin films displaying stripe domains. *J Magn Mater* 321: 806.
- Murayama Y (1966) *Micromagnetics on stripe domain films. I. Critical cases*. *J Phys Soc Japan* 21: 2253.
- Alvarez-Prado LM, Alameda JM (2004) Micromagnetism with nanowires with low out-of-plane anisotropy. *Physica B* 343: 241.
- Porrati F (2002) *Spatially varying magnetic anisotropies in ultrathin films*. Thesis (PhD), Mathematisch-Naturwissenschaftlich-Technischen Fakultät, der Martin-Luther-Universität at Halle-Wittenberg.
- Sun ZG, Kuramochi H, Mizuguchi M, Takano F, Semba Y, et al. (2004) Magnetic properties and domain structures of FeSiB thin films. *Surf Sci* 556: 33.
- Chen YT, Hsieh WH (2013) Thermal, magnetic, electric, and adhesive properties of amorphous Co₆₀Fe₂₀B₂₀ thin films. *J Alloys and Compounds* 552: 283.
- Wu D, Jin T, Lou Y, Wei F (2015) Understanding the dense stripe domains in soft magnetic film. *Appl Surf Sci* 346: 567.
- Craus CB (2003) *Magnetic Properties of Nanocrystalline Materials for High Frequency Applications*. Thesis (PhD) University of Groningen.
- Alvarez-Prado LM, Perez GT, Morales R, Salas FH, Alameda JM (1997) Perpendicular anisotropy detected by transversely biased initial susceptibility via the magneto-optic Kerr effect in Fe_xSi_{1-x} thin films and Fe_xSi_{1-x}/Si multilayers: Theory and experiment. *Phys Rev B* 56: 3306.

-
40. Hubert A, Schäfer R (1998) Magnetic domains : The analysis of magnetic microstructures. Springer-Verlag, Berlin.
41. Gayen A, Prasad GK, Mallik S, Bedanta S, Perumal A (2017) Effects of composition, thickness and temperature on the magnetic properties of amorphous CoFeB thin films. J Alloys Compounds 694: 823.
42. Das C, Mohapatra S, Vitthal GA, Perumal A (2016) Magnetic properties of single-layer and multilayer structured $\text{Co}_{40}\text{Fe}_{40}\text{B}_{20}$ thin films. Thin Solid Films 616: 126.
43. Pellegren JP, Sokalski VM (2015) Thickness and interface-dependent crystallization of CoFeB alloy thin films. IEEE Trans Magn 51: 3400903.